ISSN 2072-5981
doi: 10.26907/mrsej

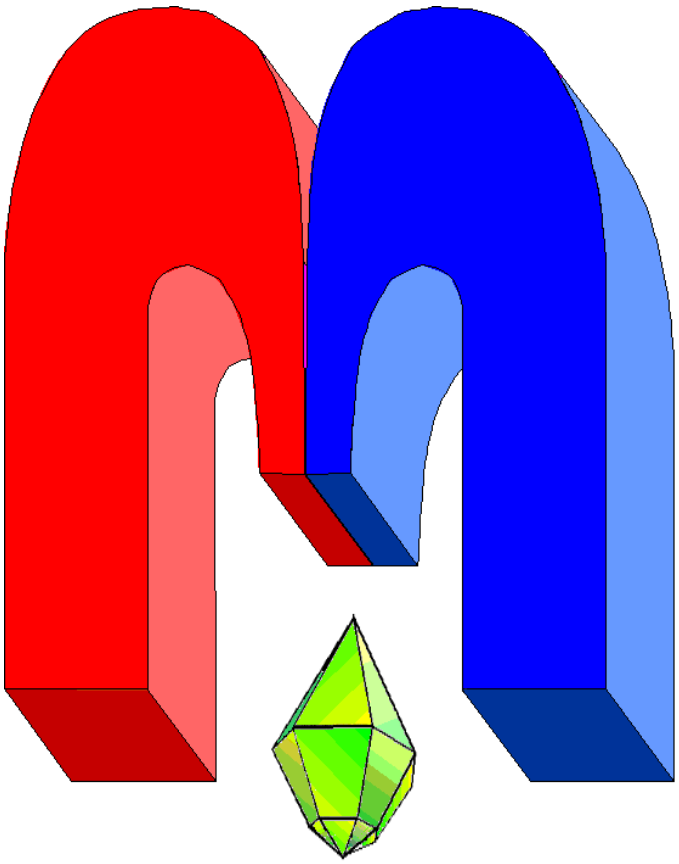

Magnetic Resonance in Solids

Electronic Journal

Volume 27
Issue 3
Article No ***25302***
1-12 pages
2025
doi: **10.26907/mrsej-25302**

http://mrsej.kpfu.ru
http://mrsej.elpub.ru

Established and published by Kazan University*
Endorsed by International Society of Magnetic Resonance (ISMAR)
Registered by Russian Federation Committee on Press (#015140), August 2, 1996
First Issue appeared on July 25, 1997

"***Magnetic Resonance in Solids. Electronic Journal***" (**MRS*ej***) is a peer-reviewed, all electronic journal, publishing articles which meet the highest standards of scientific quality in the field of basic research of a magnetic resonance in solids and related phenomena.

Indexed and abstracted by
Web of Science (*ESCI*, Clarivate Analytics, from 2015), *Scopus* (Elsevier, from 2012), *RusIndexSC* (*eLibrary*, from 2006), *Google Scholar*, *DOAJ*, *ROAD*, *CyberLeninka* (from 2006), *SCImago Journal & Country Rank*, etc.

* Address: "Magnetic Resonance in Solids. Electronic Journal", Kazan Federal University; Kremlevskaya str., 18; Kazan 420008, Russia

† In Kazan University the Electron Paramagnetic Resonance (EPR) was discovered by Zavoisky E.K. in 1944.

Short cite this: *Magn. Reson. Solids* **27**, 25302 (2025) doi: 10.26907/mrsej-25302

Correlated regimes with slow dynamics in complex oxide $LiMn_2TeO_6$

T.M. Vasilchikova[1], E.L. Vavilova[2*]

[1]Physics Faculty, Lomonosov Moscow State University, 119991 Moscow, Russia

[2]Zavoisky Physical-Technical Institute, FRC Kazan Scientific Center of RAS, 420029 Kazan, Russia

**E-mail: jenia.vavilova@gmail.com*

(received July 1, 2025; revised September 12, 2025; accepted September 16, 2025; published September 20, 2025)

Mixed-valence manganese complex oxide $LiMn_2TeO_6$ has dimeric, chain and planar structure motifs. Three Mn positions form an antiferromagnetic framework, and the fourth one ferromagnetically couples with it. The studies by nuclear magnetic resonance (NMR), AC and DC magnetization, specific heat methods show a non-trivial scenario of spin system transformation as temperature decrease. A change in correlation regimes with slow dynamics in high magnetic fields is found, as well as an unusual magnetic static phase at $T < 6$ K and $B < 5$ T. All obtained results are summarized on the magnetic phase diagram.

PACS: 76.60.-k, 75.10.Jm, 75.47.Lx, 75.85.+t, 67.57.Lm, 67.30.er

Keywords: multi-component magnetic oxides of 3d metals, correlated regimes with slow dynamics, AC magnetometry, specific heat, magnetic resonance.

1. Introduction

In recent years, studies of magnetism have focused not so much on classical magnets, where the paramagnetic regime is replaced by long-range magnetic order in a narrow temperature range, but on compounds with an extended area of slow spin dynamics and developed correlations. Of particular interest are compounds where a change in the correlation regime occurs within such a temperature range. A well-known example is low-dimensional compounds where the temperature dependencies of magnetic characteristics show the so-called "low-dimensional maximum", marking the development of strong one-dimensional or two-dimensional spin correlations [1–5]. It is important that the long-range order that arises at low temperatures is caused by three-dimensional correlations that develop in a narrow region above the transition. The ground state may not correspond to the correlations observed in the high-temperature region [6–8]. These systems often exhibit spin liquid properties, not being pure disordered systems like a pure paramagnets: it is assumed that most of them have certain "hidden order" or correlative features, which forms both their ground state and low-energy collective excitations. For frustrated systems with several competing interactions, or for inhomogeneous systems, the picture of temperature evolution can be even more complex and contain several different dynamic regimes. In some cases, it can be described in terms of dynamic phase transitions and spin fluctuation transitions [9–16]. Such a change of different dynamic regimes becomes even more pronounced in a situation for the multi-component systems. A successive change of low-frequency dynamic modes can be observed here, when the components coupled by a stronger exchange pass into a correlated state and the rest ones "adjust" to the resulting system upon cooling.

The $LiMn_2TeO_6$ is a notable example of the compound possessing the above-mentioned characteristics. Its structure consists of 4 positions of Mn ions and shows dimeric, chain and planar motifs (Figure S1 in Supplementary information), there are exchange interactions non-equal not only in magnitude, but also in sign. And, not least, the magnetic system contains manganese

ions in two different oxidation (and spin) state: Mn^{2+} and Mn^{3+} [17]. As demonstrated in our previous work [18], correlations develop at relatively high temperatures (deviation of the g-factor and growth of the electron spin resonance (ESR) line width are observed already at 100 K). The temperature dependence of the ESR line width at low temperatures shows that the dimension of the correlations is not formally determined as 3D or 2D, and takes intermediate value, expected for a complex system (Figure S2). However, the NMR relaxation shows that 3D correlations develop in the close vicinity of the transition. Phase boundary with Neel temperature $T_N = 20$ K was studied by static methods such as specific heat and DC susceptibility. The second transition at $T_2 = 14$ K is also was observed, its position shifts to higher temperatures at external magnetic field merging with the T_N boundary at 4 T. The dynamic susceptibility reveled in the frequency sensitivity of the boundary T_2. It is important to note that NMR spectra taken below the phase boundaries at $T = 12$ K indicate the same commensurate antiferromagnetic phase in all external magnetic fields up to 6.6 T. Thus, frequency-dependent T_2 boundary is not associated with the re-entrant spin glass [19–23], but indicates a crossover related to the rearrangement of the multi-component spin system. Thus, correlations and multicomponent nature seem to play an important role in the magnetism of $LiMn_2TeO_6$. The previous work [18] was devoted to the study of classical thermodynamic phase transitions in complex oxide $LiMn_2TeO_6$. During this study, we found some features in the static and especially dynamic experimental data, which indicated unusual correlated regions in the $B - T$ diagram. To obtain additional information, studies of the static and dynamic properties of the spin system were carried out over a wide range of fields and temperatures. In this paper, we carefully examine the correlated regions above T_N, and the features observed inside the ordered state. We use a combination of both static (DC susceptibility, specific heat) and dynamic experimental methods with different time resolution (AC susceptibility, NMR, ESR), which allows us to effectively distinguish and characterize various static and dynamic regimes of the magnetic system of $LiMn_2TeO_6$.

2. Experimental

The magnetic and thermodynamic properties measurements were performed by means of "Quantum Design" PPMS-9T system. Temperature dependencies of AC magnetic susceptibility χ_{AC} were measured at the magnitude of alternating magnetic field 1 Oe in the frequency range 1–10 kHz. Specific heat measurements were carried out by a relaxation method. The data were collected at 0–9 T in the range 2–30 K.

The ^{7}Li ($I = 3/2$) nuclear magnetic resonance (NMR) experiments were performed using pulse solid-state NMR spectrometer "Tecmag" on ^{7}Li nuclei in the external field ranges around 2 and 6 T. Spectra were obtained by point-by-point integration of the spin echo intensity during field sweeping. The observed ^{7}Li NMR spectrum is a superposition of the signals from all lithium nuclei in powder sample. The spin-lattice relaxation rate T_1^{-1} was measured with saturation recovery and stimulated echo pulse sequence. Due to the strong inhomogeneous line broadening and the presence of unresolved quadrupole satellites, the stretch exponential dependencies $M = M_0(1 - \exp[(-\tau/T_1)^b])$, $(M = M_0 \exp[(-\tau/T_1)^b])$ was used to approximate the recovery (decay) curves of the magnetization M (here τ is the interpulse delay). So-called stretch coefficient $0.75 < b < 0.9$ characterizes in this case the inhomogeneity and effective dimensionality of the local magnetic environment of the lithium nucleus. In the analysis and construction of the model, both new results and some of the data published in our previous work [18] were used.

3. Results and discussion

AC susceptibility measurements at high fields demonstrate that the phase line $T_2(T, B)$, which marks the frequency-dependent transition within the ordered phase in low fields, is not limited to the region of static ordering, but continues above the Neel temperature as field increases. The position of the maximum on $\chi'(T)$ increases monotonically with temperature as the field increases, while the feature itself remains frequency-dependent. The maximum on $\chi'(T)$, observed at 7 T at a temperature of $T \sim 25$ K is shown as an example in Figure 1. Formal analysis within a critical slowing down model [24] developed for spin glass freasing allows us to estimate the correlation time as 10^{-7} s (see the inset in Figure 1 and the caption to Figure 1). This means that the frequency of spin fluctuations in the temperature vicinity of the T_2 maximum is comparable with the nuclear magnetic resonance frequency.

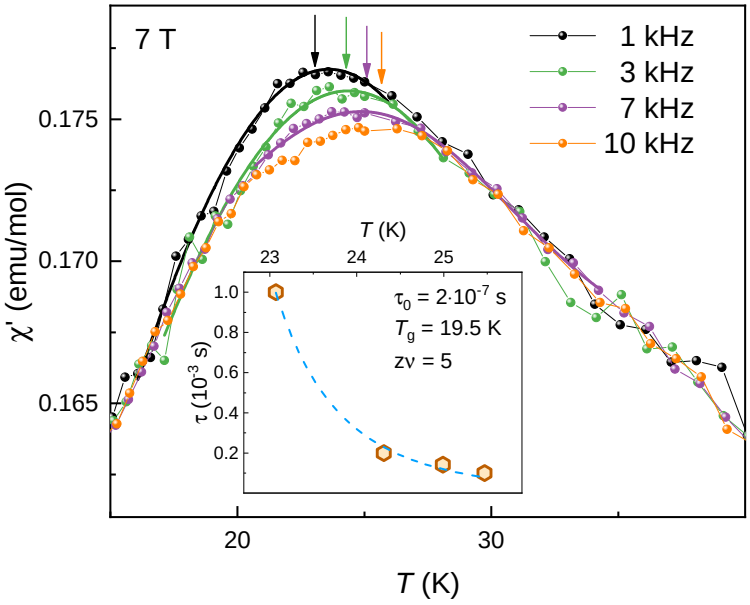

Figure 1. Temperature dependencies of the real χ' part of AC magnetic susceptibility in $LiMn_2TeO_6$, at various frequencies in the range of 1–10 kHz. Inset: critical analysis of the peak position using the formula $\tau(T_f) = \tau_0(T_f/T_g - 1)^{-z\nu}$ (where τ_0 is the microscopic spin flip time, T_f is the frequency-dependent freezing temperature at which the maximum relaxation time ($\tau = 1/\omega$) of the system corresponds to the measurement frequency, T_g is the freezing temperature (at $\omega \to 0$), and $z\nu$ is the critical exponent.

Indeed, NMR experiments allows us to distinguish different regimes when crossing a conditional boundary, marked by dependence $T_2(T, B)$ (see Figure 2). Recall that NMR parameters can provide information on the local susceptibility at the position of the resonating nucleus. The line shift K is proportional to the local static susceptibility at frequencies lower than the resonance frequency and zero wave vector ($K \sim A_{\|}\chi_{\text{loc}}(\mathbf{q} = 0)$). In the paramagnetic region, the spin-lattice relaxation rate divided by the temperature is proportional to the imaginary part of dynamic susceptibility χ'', which depends on the frequency and wave vector $(T_1T)^{-1} \sim \chi''(\mathbf{q}, \omega)/\omega$. In the temperature range close to T_2, both static and dynamic local susceptibilities demonstrate some specific features. The static local susceptibility K has a pronounced maximum near the temperature T_2 (Figure 2a), which is typical for low-dimensional systems (including FM dimers linked by weak AFM interaction [25]) and usually points to the transition to a strongly correlated regime. The development of correlations and the slowing

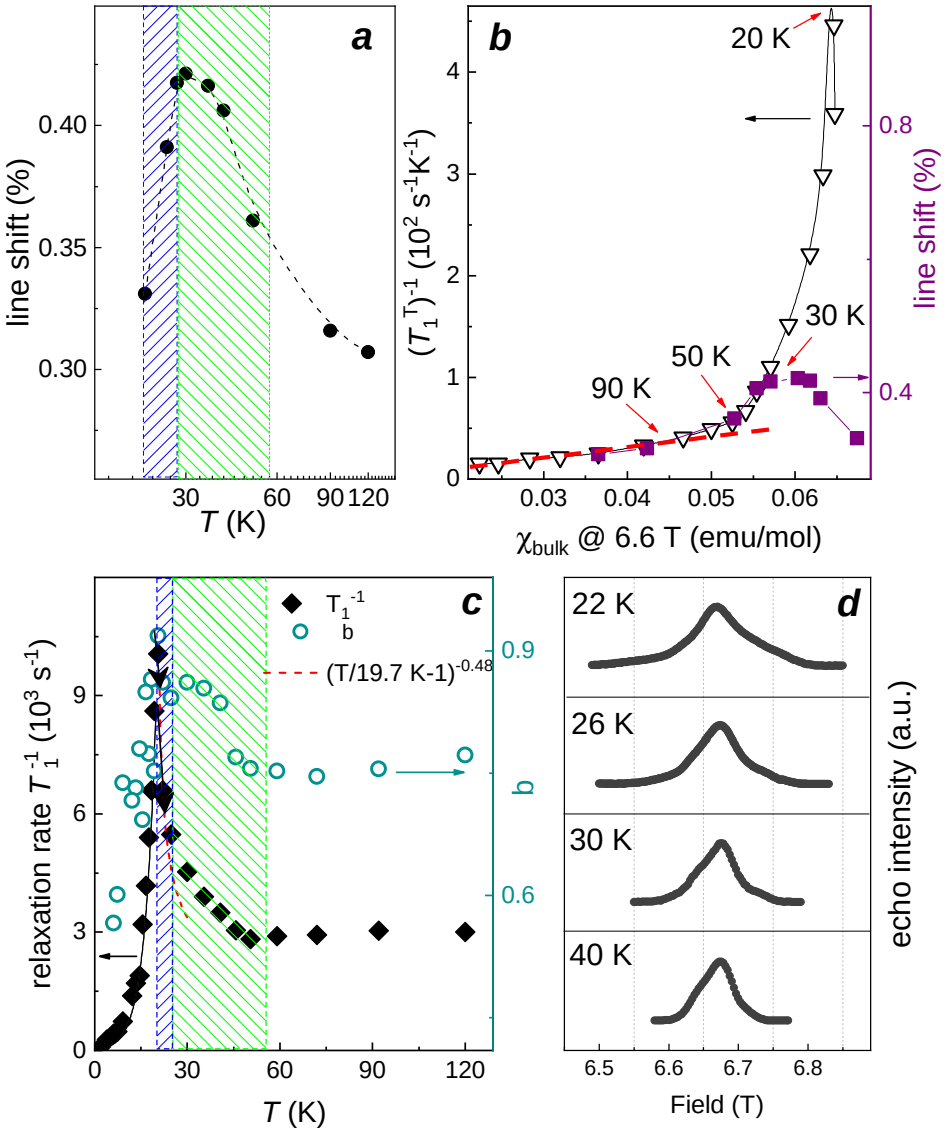

Figure 2. (**a**) Temperature dependence of the line shift taken from the maximum of the magnitude. Dashed line is a guide for eyes. (**b**) Local static (open triangles) and dynamic (violet squares) susceptibility measured by NMR at 6.6 T, plotted as a function of the bulk static susceptibility χ_{bulc} measured at 6.6 T. The red dashed line denotes the linear dependence (see text). (**c**) Temperature dependence of the relaxation rates (black diamonds) and stretch exponent coefficient (green open circles) taken at 6.6 T. (**d**) ^{7}Li NMR spectra obtained in the correlated region at 6.4 T $> B >$ 6.9 T. The blue and green shaded regions correspond to different correlation regimes (see text).

down of spin fluctuations can be clearly traced by plotting the dependence of local static (K) and local dynamic $(T_1T)^{-1}$ susceptibility on the static bulk susceptibility χ_{bulk}, obtained in the same magnetic field (Figure 2b). The state of spin system between T_N and T_2 in high fields is definitely not a spin glass: the curves of DC susceptibility and magnetic specific heat do not contain visible features here, the width of the NMR spectrum remains very narrow compared to the static state, and the relaxation peak, marking the slowing down of fluctuations below the NMR frequency, clearly correlates with T_N, not T_2. Consequently, we are not dealing with a static phase, but with a strongly correlated state with slow spin fluctuations, with a different

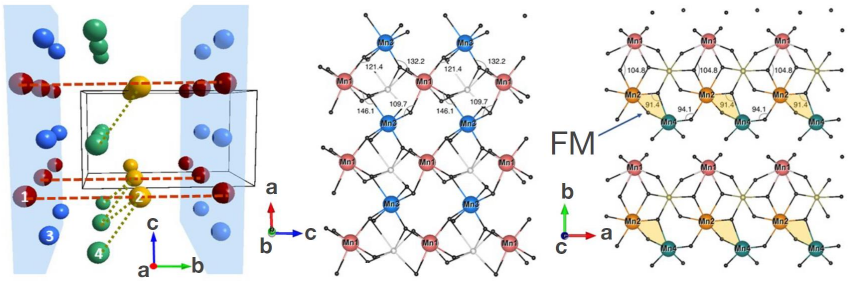

Figure 3. Bonds and bond angles between manganese ions in the structure of $LiMn_2TeO_6$. Different Mn ion positions are marked by color: red circus are Mn1 ions, yellow circus are Mn2, blue circus are Mn3 and green circus are Mn4. Only Mn ions are shown in left panel, only Mn and O ions are shown in central and right panel. The small light grey and light yellow balls are Li and Te ions respectively.

character of anisotropy than above T_2. The development of the correlations becomes noticeable at temperatures below ~ 90 K, when the local susceptibility ceases to be linear to bulk. Below ~ 50 K, the dependence of local susceptibility on the **q**-vector becomes significant, which leads to a divergence between $(T_1T)^{-1}(T)$ and $K(T)$. The relaxation rate increases noticeably in this temperature range (green area in Figure 2c) and the stretch exponent coefficient changes drastically indicating the emerging anisotropy of the correlated spin system geometry. At the same time, the stretch coefficient increases, which is not typical for AFM-correlated behavior. We also note that $T \sim 50$ K can serve as an approximate boundary for the disappearance of the ESR signal in the X-range with decreasing temperature (see Figure S2). Taking into account the narrowness of the temperature range where the NMR relaxation parameters change, we can consider the scenario of a spin-fluctuation transition near 50 K. The multicomponent and heterogeneous nature of the system, containing both manganese ions with different spin values and several of their structural positions, can provide a sharp change in the rate and anisotropy of spin fluctuations when the temperature becomes lower than any interaction. Additional studies are required to clarify the scenario of the spin-system transformation in this temperature range.

The behavior of the dynamic NMR characteristics in the critical region near the AFM transition also depends strongly on the magnetic field. In contrast to weak fields, the description with the critical index [18], typical for 3D ordering (red line in Figure 2c), can be detected at 6.6 T only in the very close vicinity of the Neel temperature, and above T_2 the dependence deviates towards 2D behavior.

Therefore, we can clearly distinguish between two temperature regions with strong correlations: 20–25 K with 3D AFM correlations (shaded blue in Figure 2) and 25–50 K where spin correlations have lower dimensionality and non-AFM character (shaded green in Figure 2). It means the effective dimension of the interactions that provide these spin correlations. These are the spin interactions that "come into play" from larger to smaller as the temperature decreases. Finally, the most striking evidence of a change in the spin system effective geometry is the pronounced transformation of NMR powder line shape occurring at about 25 K (Figure 2d): the low-field shoulder of the line, expressed at $T > 30$ K, disappears with decreasing temperature and at $T < 25$ K the high-field shoulder begins to grow. In concentrated paramagnets, the NMR line shape mainly reflects the distribution of internal magnetic fields at the positions of the sensor nucleus produced by the electron spin system via indirect hyperfine coupling. There-

fore, the change of the spectral shape in the comparably narrow temperature range indicates a transformation of the effective hyperfine tensor on Li nucleus caused by the development of correlations and a dramatic slowdown in the fluctuations of the electron spins of manganese.

The increase of temperature T_2 with the field may indicate the presence of ferromagnetic interactions in this system. A careful analysis of the magnetic lattice structure of studied compound allows highlighting several motifs (Figure 3):

1. AFM bonded Mn1-Mn3 ions form the layers in *ac* plane.

2. These layers connected through Mn2 ions build up a three-dimensional framework with all bond angles greater than 100 degrees.

3. Mn4 ions are coupled only to Mn2 ions with Mn-O-Mn bond angles $\sim$ 90 degrees, i.e. Mn4-Mn2 bond is ferromagnetic.

Therefore, we propose the following scenario: in low fields, an antiferromagnetic transition takes place within the Mn1-Mn2-Mn3 ions system. The Mn2-Mn4 component remains dynamic, which is reflected in the AC susceptibility data. It adapts to the main system at slightly lower temperatures ($T_2 = 14$ K) resulting in the formation of the AF1 phase. Tiny disorder or defects in the crystal structure are enough to cause such adjustment to occur in the form of a crossover with frequency-dependent features. The application of external magnetic field is favorable for the ferromagnetic interaction in Mn2-Mn4 pair, and the T_2 boundary shifts upward in temperature. At $B > 4$ T, the growth of these FM correlations outpaces the development of the static AFM order. The AC and NMR data show a remarkable slowdown of the fluctuations of the correlated Mn2-Mn4 ion spins below 40 K. It should be noted that the formation of ferromagnetic dimers is not occur, since there is no jump in magnetization. At high external magnetic fields, the formation of antiferromagnetic order happens in the background of these correlations.

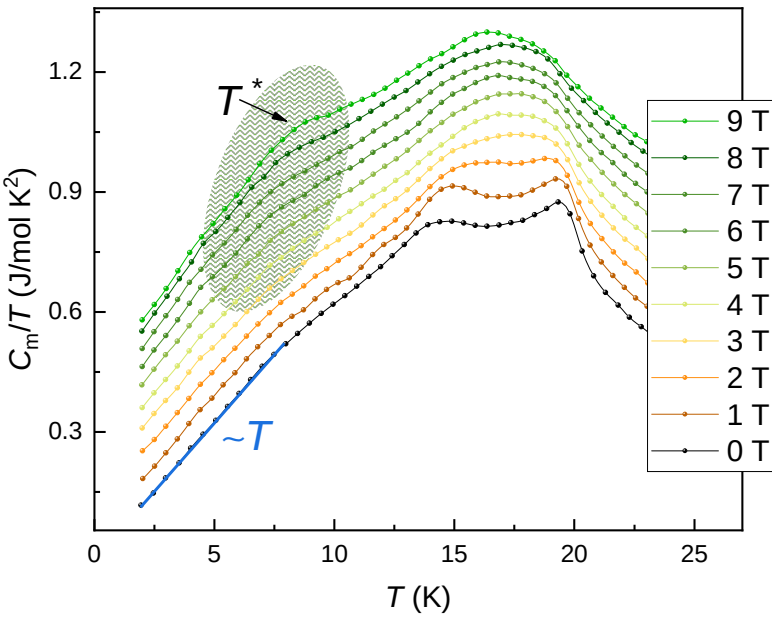

Figure 4. The magnetic specific heat C_m/T dependencies at various external magnetic fields. The blue line is the result of the spin-wave theory fit. The region of the T^* anomaly corresponding to the transition to low-T - high-B phase is marked in green.

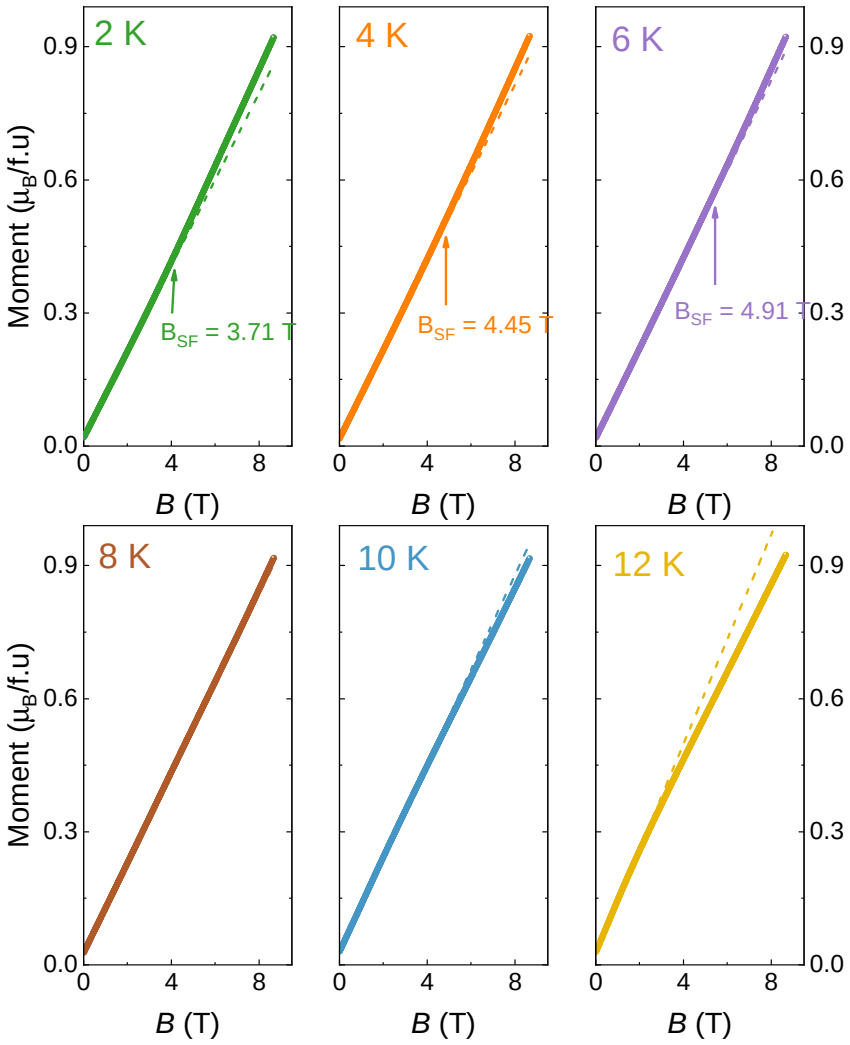

Figure 5. Field dependence of magnetization taken in different temperatures. Dashed lines show the linear approximation based on the low field experimental points.

The formed spin structure seems to be not equilibrium enough to become the ground state in high fields. Therefore, additional transformations of the magnetic structure can be expected with a further temperature decrease. Weak but noticeable anomalies at a temperature that we will designate as T^* on the temperature dependencies of the magnetic specific heat C_m in fields of 5–9 T (Figure 4) can be attributed to this spin reorientation process.

In addition, a kink is observed in the field dependencies of magnetization for $T < 6$ K, which usually corresponds to the reorientation transition of AFM structure in the external field (Figure 5, upper panel). The temperature dependencies of these features limit the area of the phase diagram in high fields at low T ("pink" in Figure 6). In order to make sure that the magnetic structure in this region is really different from other ordered regions, we measured the NMR spectra at 4 points within the ordered state (Figure 7). The spectra at points **b** – **d** ("green") have the same stepped shape, slightly shifting with increasing field, which is typical for collinear AFM state [26]. Step widths are set by the local fields at the lithium positions, which are found to be the same in all three $B-T$ points. The smoothed shape and broadening of the spectrum peak at spectrum **a** - "pink") a indicates that the distribution of local fields on lithium positions in this case is not discrete, but continuous. Therefore, it can be assumed that the spin

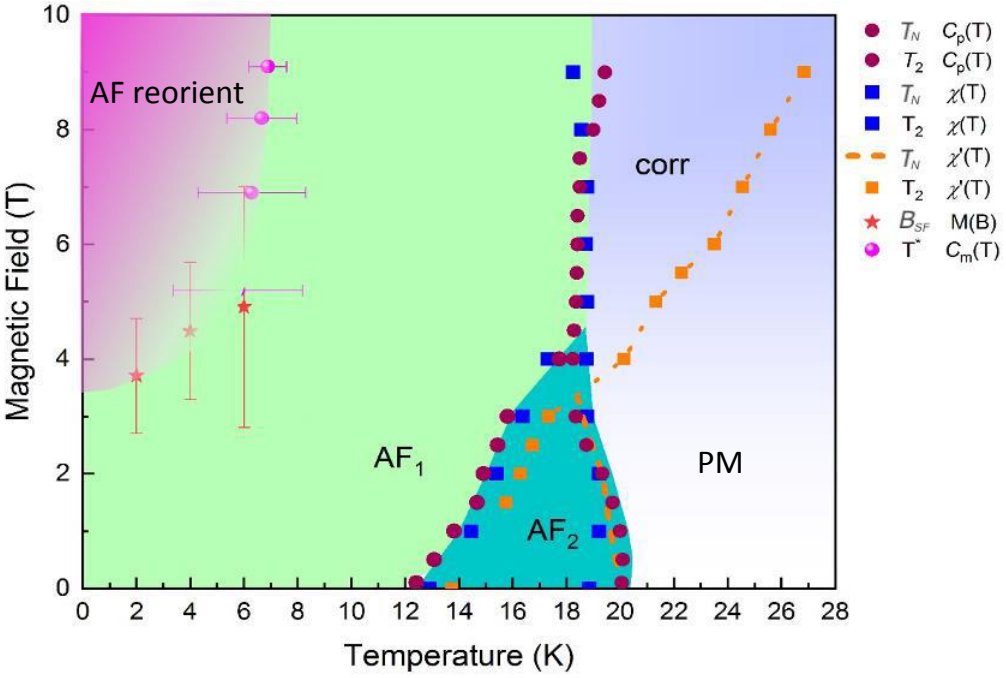

Figure 6. Phase diagram for $LiMn_2TeO_6$ with correlated regions above T_N.

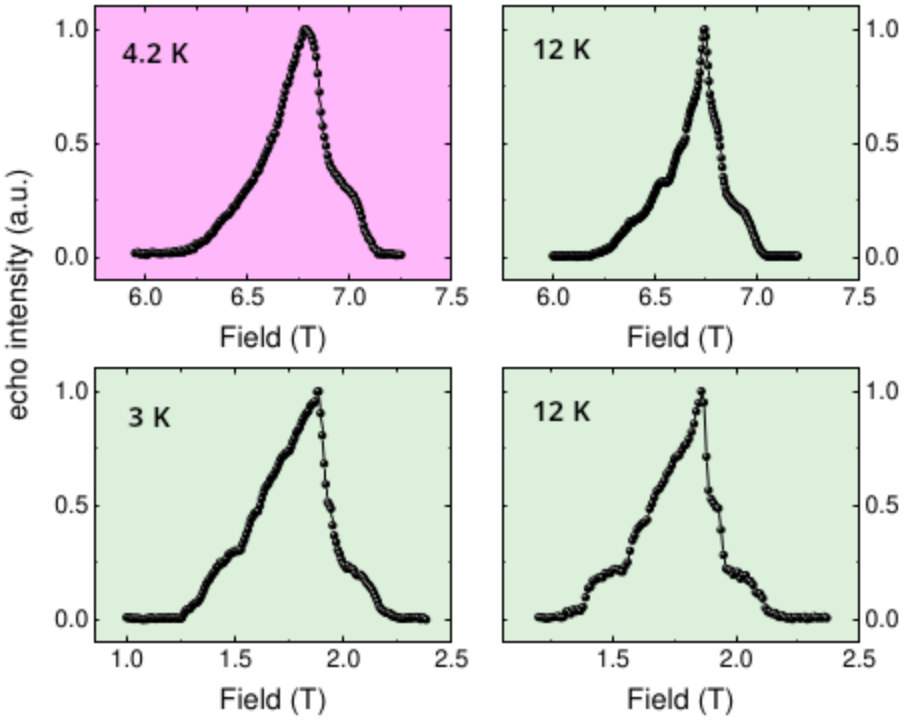

Figure 7. ^{7}Li NMR spectra taken in AFM region of phase diagram (b–d) and in low T-high B area (a) (colors correspond to phase diagram at Figure 6).

structure in this field and temperature region is different and, most likely, incommensurate. An analysis of $C_m(T)$ in terms of the spin-wave approach [27,28] indicates the presence of 2D AFM magnons at low temperatures (blue solid lines in Figure 4) in low and high fields. This suggests

a significant role of antiferromagnetic Mn1-Mn3 planes in both the "green" and "pink" phases. Neutron diffraction study will be useful for precise spin structure determination.

4. Summary

The present paper is devoted to a high-field study of the correlated region above T_N and a new low-temperature phase within the static region. Here, static and quasistatic methods ($M(B)$, $C_m(T)$, $\chi'(T,B)$) give us the boundaries of phases and correlated regions, and NMR allows us to prove that the state of the spin system there is actually different. In $LiMn_2TeO_6$, due to its multicomponent nature, the temperature transformation to the ground state occurs in several steps. Depending on the balance of temperature, main exchanges and the external magnetic field energy, a consistent mutual adjustment of different magnetic subsystems is observed. One of the subsystems forms an antiferromagnetic framework and couples with the other one by ferromagnetic exchange. For this reason, in low fields (up to 4 T), the adjustment occurs via a crossover within the already established AFM order. In high field supporting the ferromagnetic interaction, a change in correlated regimes with slow dynamic precedes the Neel order. The non-equilibrium of the obtained static state causes an additional metamagnetic transition at $T < 6$ K and $B > 5$ T. On the basis of our experimental data, we assume that the spin structure in this region seems to be incommensurate.

5. Acknowledgments

The authors are thankful to Dr. V. Nalbandyan (SFU, Russia) for the sample synthesis. E.V. would like to thank the financial support from the government assignment for FRC Kazan scientific Center of RAS. T.V. acknowledges for the support of the conducted research by the Russian Science Foundation, project 25-12-00028.

References

1. Mikeska H., Kolezhuk A., *"One-dimensional magnetism,"* in *Quantum Magnetism. Lecture Notes in Physics, vol 645*, edited by Schollwöck U., Richter J., Farnell D., Bishop R. (Springer, Berlin, Heidelberg, 2004) pp. 1—–83.

2. Johnston D., Kremer R., Troyer M., Wang X., Klümper A., Bud'ko S., Panchula A., Canfield P., *Phys. Rev. B* **61**, 9558 (2000).

3. Vasiliev A., Volkova O., Zvereva E., Markina M., *npj Quant. Mater.* **3**, 18 (2018).

4. Schmitt M., Janson O., Golbs S., Schmidt M., Schnelle W., Richter J., Rosner H., *Phys. Rev. B* **89**, 174403 (2014).

5. Balents L., *Nature* **464**, 199–208 (2010).

6. Heinrich M., Krug von Nidda H.-A., Loidl A., Rogado N., Cava R. J., *Phys. Rev. Lett.* **91**, 187206 (2003).

7. Klyushina E. S., Lake B., Islam A. T. M. N., T.Park J., Schneidewind A., Guidi T., Goremychkin E. A., Klemke B., Maensson M., *Phys. Rev. B* **96**, 214428 (2017).

8. Iakovleva M., Janson O., Grafe H.-J., Dioguardi A. P., Maeter H., Yeche N., H.-H.Klauss, Pascua G., Luetkens H., Moeller A., Buechner B., Kataev V., Vavilova E., *Phys. Rev. B* **100**, 144442 (2019).

9. Miyashita S., *Proc. Jpn. Acad. Ser. B* **86**, 643 (2010).

10. Jafari R., *Sci. Rep.* **9**, 2871 (2019).

11. Bogoslovskiy N., Petrov P., Averkiev N., *JETP Lett.* **114**, 347–353 (2021).

12. Porta S., Cavaliere F., Sassetti M., Traverso Ziani N., *Sci. Rep.* **10**, 12766 (2020).

13. Demishev S., *Phys. Usp.* **67**, 22 (2024).

14. Demir Vatansever Z., *Phys. Rev. E.* **106**, 054143 (2022).

15. Wong C. Y., Cheraghi H., Yu W. C., *Phys. Rev. B.* **108**, 064305 (2023).

16. Ettori F., Coupé T., Sluckin T., Puppin E., Biscari P., *Entropy* **26**, 120 (2024).

17. Pospelov A., Nalbandyan V., Serikova E., Medvedev B., Evstigneeva M., Ni E., Lukov V., *Solid State Sci.* **13**, 1931–1937 (2011).

18. Vasilchikova T., Vavilova E., Salikhov T., Nalbandyan V., Dengre S., Sarkar R., H.-H. Klauss A. V., *Materials* **15**, 8694 (2022).

19. Sato T., Ando T., Ogawa T., Morimoto S., Ito A., *Phys. Rev. B* **64**, 184432 (2001).

20. Niidera S., Matsubara F., *Phys. Rev. B* **75**, 144413 (2007).

21. Motoya K., Shapiro S., Muraoka Y., *Phys. Rev. B* **28**, 6183 (1983).

22. Clark J., Tan X., Garlea V., Arico A., Ramirez A., Yannello V., C.M.Thompson, Kovnir K., Shatruk M., *Phys. Rev. Materials* **4**, 074412 (2020).

23. Matsubara F., Niidera S., *J. Magn. Magn. Mater.* **310**, e515 (2006).

24. A.Mydosh J., *Rep. Prog. Phys.* **78**, 052501 (2015).

25. Borras-Almenar J., Coronado E., Curely J., Georges R., Gianduzzo J., *Inorg. Chem.* **33**, 5171 – 5175 (1994).

26. Yamada Y., Sakata A., *J.Phys. Soc. Jpn.* **55**, 1751–1758 (1986).

27. Carlin R. L., *Magnetochemistry* (Springer-Verlag, Berlin, Germany, 1986).

28. de Jongh L. J., Miedema A. R., *Adv. Phys.* **23**, 1–260 (1986).

29. Kawasaki K., *Phys. Lett. A* **26**, 543 (1968).

30. Mori H., Kawasaki K., *Progress of Theoretical Physics* **28**, 971–987 (1962).

31. Huber D. L., *Phys. Rev. B* **6**, 3180 (1972).

32. Richards P., *Solid State Commun.* **13**, 253–256 (1973).

33. Anders A., Volotski S., *J. Magn. Magn. Mater.* **31-34**, 1169–1170 (1983).

Supporting information

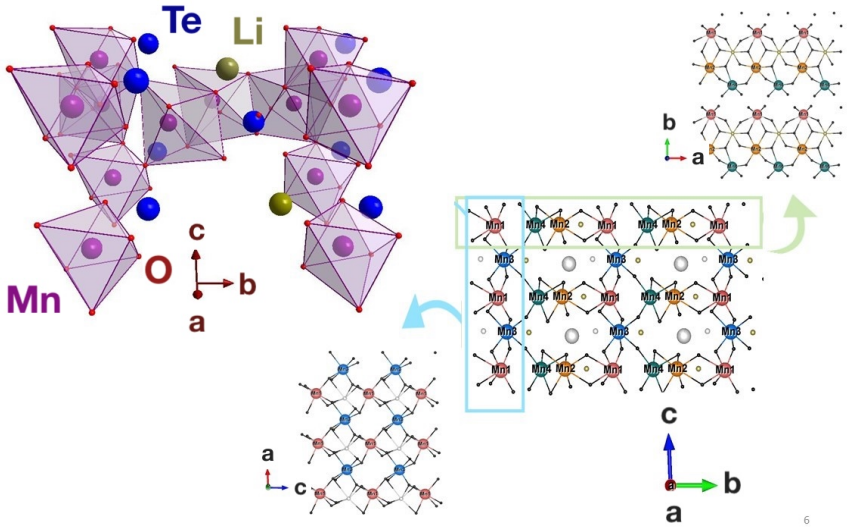

Figure S1. Low-dimensional motifs of manganese ion arrangement in the crystal structure of $LiMn_2TeO_6$.

Over the entire temperature range studied, the ESR spectra exhibit a single resonance line attributed to overlapping signals from Mn^{2+} and Mn^{3+} ions. As the temperature decreases, the signal rapidly broadens and eventually disappears below 40 K. Within the framework of the Kawasaki-Mori-Huber theory [29–31], the temperature change in the line width ΔB can be described as

$$\Delta B^* + A \cdot [(T_N^{ESR})/(T - T_N^{ESR})]^{\beta}, \tag{S1}$$

here A is an empirical parameter, ΔB^* is the high-temperature limiting value of the linewidth, T_N^{ESR} is the temperature of the order-disorder transition and β is a critical exponent. A least-squares fitting of the experimental data (the red line in Figure S1) reveals that the value of $T_N^{ESR} = 21 \pm 2$ K is close to the Neel temperature and critical exponent $\beta = 0.70 \pm 0.1$ K indicates the presence of quasi-2D nature [32] of the exchange correlations in $LiMn_2TeO_6$. The curves calculated for 3D ($\beta = 0.33$, green line) and pure 2D correlations ($\beta = 1.5$, violet line) are not consistent with the experimental data.

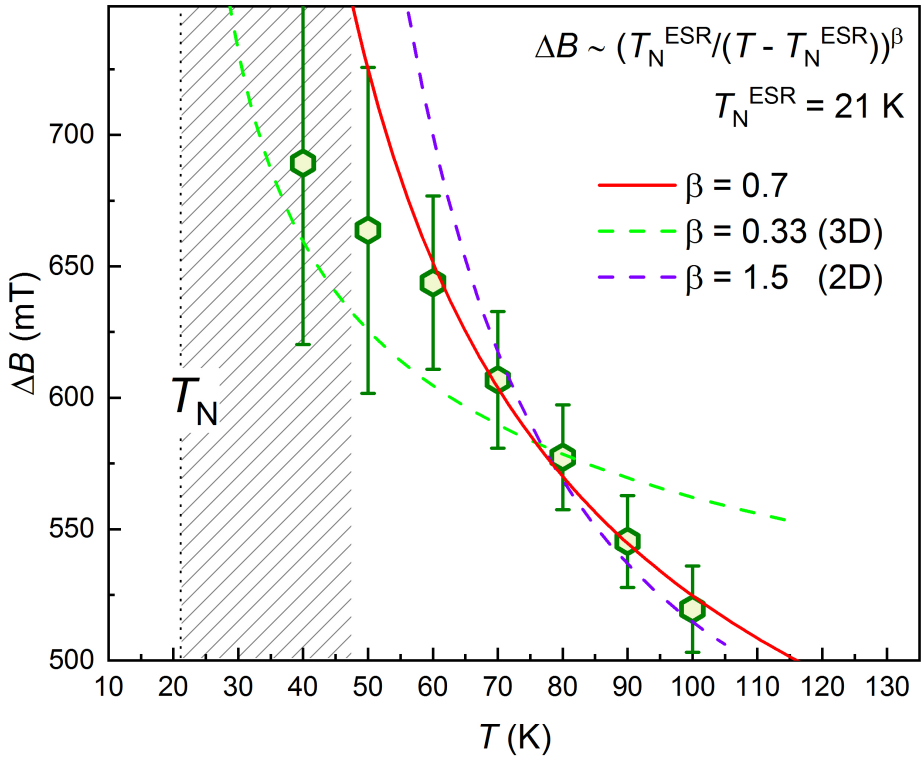

Figure S2. The temperature dependence of ESR linewidth ΔB (open symbols). The solid curves correspond to the temperature dependence of the linewidth within the framework of classical critical behavior with different values of β [32, 33].